Vertical distributions of Cs-137 in soils: a meta-analysis

Marianna Jagercikova, Sophie Cornu, Christine Le Bas, O. Evrard

SOILS, SEC 2 • RESEARCH ARTICLE

Vertical distributions of ^{137}Cs in soils: a meta-analysis

Marianna Jagercikova • Sophie Cornu • Chrsitine Le Bas • Olivier Evrard

M. Jagercikova • S. Cornu (✉)

INRA, UR1119 Géochimie des Sols et des Eaux, 13100 Aix en Provence, France e-mail: Sophie.Cornu@aix.inra.fr

C. Le Bas

INRA, US 1106 Infosol, 45075 Orléans, France

O. Evrard

LSCE, UMR8212 CEA-CNRS-UVSQ, Domaine du CNRS, 91198 Gif-sur-Yvette Cedex, France

(✉) **Corresponding author:**

Sophie Cornu

Tel: +33 ø4 42 97 17 96

Fax: +33 ø4 42 90 85 17

e-mail: Sophie.Cornu@aix.inra.fr

Abstract

Purpose. The vertical distribution of ^{137}Cs – an artificial fallout radionuclide – is controlled by soil characteristics and processes that may differ among soil groups. The application of a single modelling approach to large number of soil profiles provides an original contribution to the literature and allows for comparison between these different soil groups.

Materials and methods. In order to quantify ^{137}Cs migration in soils, we compiled and modelled depth-distributed data documented in the literature between 2000–2012. The resulting database comprised ninety-nine ^{137}Cs profiles sampled in fourteen soil groups of the World Reference Base (WRB) classification (FAO 1998) under different land uses or covers and collected at various geographical locations in the Northern hemisphere between 1992 and 2007.

Results and discussion. The ^{137}Cs profiles were classified in seven different categories according to the shape and location of radiocaesium peak. Depth of the latter ranged between 0 and 12 cm (median of 2 cm) and maximal penetration of cesium reached from 12 to 60 cm. The ^{137}Cs depth distributions in these soils were fitted using a diffusion-convection equation to allow comparison between different soil groups. Diffusion coefficients ranged from 0.02 to 4.44 $cm^2\ yr^{-1}$ in soils (median of 0.64 $cm^2\ yr^{-1}$); and convection velocities varied from 0 to 0.74 cm yr^{-1}(median of 0.1 cm yr^{-1}). The model underestimated ^{137}Cs concentrations by a median value of 1.9% of the total inventory in soil samples collected below 13 cm depth.

Conclusions. Global ^{137}Cs penetration velocities ranged from 0.05 to 0.76 cm yr^{-1} (median of 0.28 cm yr^{-1}) over a 25-year period. In future, the model could be improved to better simulate deep penetration of Cs. Our results showed that modelling ^{137}Cs depth profile with a diffusion-convection equation allowed estimating the bioturbation and clay translocation velocity in a certain number of soil groups. This quantification is crucial as these processes partially control the development of soil surface characteristics and several soil services.

Keywords Bioturbation • Clay translocation • Diffusion-convection equation • Fallout radionuclides • Numerical modelling • Pedogenesis

1 Introduction

Ceasium-137 is characterised by a strong affinity for fine soil particles and is therefore widely used to quantify soil erosion at the plot and hillslope scales (Ritchie and Ritchie 2007), but it is also employed to quantify the relative contribution of sources delivering sediment to rivers (Ben Slimane et al. 2013). However, its ability to trace vertical transfers of solid matter in soils was much less investigated. Despite the importance of these transfers in controlling the soil surface characteristics, the occurrence and the velocity at which those transfers operate are still poorly understood and quantified. To this end, measurement of tracers that are strongly bound to the solid phase and that were absent from the parent material before the start of pedogenesis along soil profiles could provide relevant information to improve our knowledge on those processes.

Although some limitations to this method exist (e.g. Parsons and Foster 2011), caesium-137 fulfils both conditions. It was released into the atmosphere by the nuclear weapon tests or, more recently, by nuclear accidents like Chernobyl or Fukushima. Soils may therefore be considered as free of this isotope prior to the first nuclear weapon tests in 1953. During the nuclear weapon tests, from the 1950s to the 1970s, ^{137}Cs was mixed in the stratosphere and its deposition pattern to the terrestrial surface, referred to as global fallout, reflects the atmospheric circulation and its latitude-dependence (UNSCEAR 1982). In contrast, ^{137}Cs atmospheric deposits after nuclear accidents displayed locally heterogeneous spatial patterns, mostly depending on the weather conditions that prevailed shortly after the emissions (Chartin et al., 2013; Korsakissok et al. 2013). As a result of the combination of wet and dry fallout, ^{137}Cs is delivered to the soil surface, and it may then migrate in depth at a rate depending on processes controlling this transfer and soil characteristics.

These characteristics control the fixation of ^{137}Cs on solid phases. Caesium-137 was shown to be fixed on soil constituents such as micaceous clay minerals (Tamura and Jacobs 1960;

79 Sawhney 1972; Konoplev et al. 1996; Bunzl et al. 1998), bearing Frayed Edge Sites (FES)
80 which are specific sites for caesium sorption (Cremers et al. 1988). According to
81 Vandenbroek et al. (2012), surface layers of most soils found across the world were shown to
82 have a high selectivity for caesium adsorption, with the exception of Oxysols, Podzols and
83 Andosols that are depleted in micas. Regarding the other soil types, Gil-Garcia et al. (2009)
84 found high solid/liquid distribution coefficients (K_d) for caesium with mean K_d values of 530
85 L kg^{-1}, 5 500 L kg^{-1} and 3 500 L kg^{-1} for sandy, clayey and loamy soils respectively. Under
86 these conditions, transport of caesium in dissolved form may be considered negligible after
87 the initial fixation of this radionuclide onto mineral soil particles (Elshamy et al. 2007; Jarvis
88 et al. 2010; Matisoff et al. 2011). Consequently, over the long-term, radionuclides are mainly
89 transported along hillslopes with soil particles (Müller-Lemans and van Dorp, 1996; Turner et
90 al. 2006). In this context, the presence of artificial fallout radionuclides in depth can be
91 interpreted as resulting from a particle-borne transfer due to clay migration or to a physical
92 mixing by turbation including bioturbation processes (Müller-Lemans and van Dorp 1996;
93 VandenBygaart et al. 1998; Ireson and Butler 2009). Nevertheless organic soils containing
94 more than 20 % of organic matter were shown to have a relatively lower K_d value (mean of
95 270 L kg^{-1}) (Gil-Garcia et al. 2009). In these soils, a significant contribution of solute transfer
96 of ^{137}Cs that may be associated with DOC cannot be ruled out (AIEA 2010).
97 Finally, the relatively short half-life of ^{137}Cs ($T_{1/2}$=30 yr) is particularly relevant for
98 investigating processes occurring at decadal scales (Kaste et al. 2007). Although soil
99 formation occurs over much longer periods, individual pedological processes may be
100 characterised by temporal variations with a succession of active and inactive periods
101 throughout the entire story of soil development. The use of ^{137}Cs as a tracer provides therefore
102 a relevant tool to understand and quantify those variations during the last 50 years.
103 Most approaches that aimed to quantify the migration velocities of fallout radionuclides in

104 soils solved the diffusion-convection equation (e.g. Bossew and Kirchner 2004; Schuller et al.
105 2004; Schimmack and Márquez 2006), using either analytical or numerical solutions (Smith
106 and Elder 1999; Bunzl et al. 2000; Bossew and Kirchner 2004).
107 In this study, we aimed at quantifying the kinetics of vertical transfers of ^{137}Cs in soils
108 depending on their characteristics and the relative contribution of processes controlling this
109 transfer in soils. To this end, we modelled the vertical distributions of ^{137}Cs fallout along soil
110 profiles documented in the literature.
111
112 **2 Materials and methods**
113 2.1 Database description
114 The database compiles 99 profiles with detailed evolution of ^{137}Cs activities with depth
115 retrieved from 17 publications published before 2013 (Table 1, detailed information is
116 provided in the Electronic Annex A). We restricted our work to the investigations mentioning
117 the soil group of the studied profiles. This reduced considerably the amount of relevant
118 studies among the hundreds of studies dedicated to ^{137}Cs in soils that have been continuously
119 published since the mid-1990s (Ritchie and Ritchie 2007). Land use or cover, altitude, annual
120 precipitation, sampling date and pedological data such as pH and organic matter content were
121 compiled when available. The depth of maximum ^{137}Cs concentration and the maximum
122 depth reached by ^{137}Cs were also collected.
123 In these studies, ^{137}Cs data were expressed in different units: Bq kg^{-1} (direct measurement of
124 ^{137}Cs activity in gamma spectrometry - 85 % of observations), Bq cm^{-3} (^{137}Cs activity per
125 volume of soil, which requires multiplying the values in Bq kg^{-1} by the bulk density – 2 % of
126 observations), Bq cm^{-2} (inventory per layer, which requires multiplying the values in Bq cm^{-3}
127 by the sample thickness – 7 % of observations), or percentage of the total inventory % Bq cm^{-}
128 ^{2} (inventory per layer divided by the total inventory - 6 % of observations). All ^{137}Cs data

129 were therefore converted into Bq cm^{-3} to facilitate modelling. Several pedotransfer functions
130 exist to estimate soil bulk density (De Vos et al. 2005). However, they are generally based on
131 the measurements of organic matter content or particle-size distributions and these data were
132 not available in most of the compiled studies. We therefore derived a relationship between
133 this parameter and the soil depth from the values available for 13 soil profiles.). However,
134 We determined the duration between soil sampling and publication (mean of four years with a
135 standard-deviation of 1 year). Therefore, when not available (6 profiles), the sampling date
136 was estimated as the publication date minus 4 years.
137 Soil groups were given according to different classifications (WRB in 38 % of studies (FAO,
138 1998); Soil Taxonomy in 36 % of studies (Soil Survey Staff 1999) and national classification
139 systems in the remaining studies). To allow for comparison, all soil groups were reclassified
140 according to the WRB system (FAO 1998). Among the 30 main soil groups of the WRB
141 classification, only 14 soil groups were represented in the database (Table 1).
142 The studies were conducted in 12 countries from the Northern Hemisphere that were
143 submitted to different levels of ^{137}Cs contamination due to the Chernobyl accident, which
144 resulted in a large variability in ^{137}Cs inventories (Table 1).
145 Soil profiles were collected under different land uses or covers, i.e. grassland (56 % of the
146 cases), woodland (25 % of the cases), peatland (2% of the cases), cropland (4% of the cases),
147 and land use or cover was not specified in 13 % of the cases. In the latter case, the sites were
148 described as undisturbed and we hypothesised that they were under grassland.
149 Most studies restricted sampling to the uppermost 20-cm layer (87 %). However, in 79 % of
150 the cases, the deepest sample had ^{137}Cs non-null concentration. The inventories estimated by
151 the authors were therefore probably underestimated.
152 In some studies, only three samples were analysed along the profile. The modelling approach
153 was therefore not applicable to such a small number of samples and these soil profiles were

154 removed from further analysis (16 profiles). We did not model ^{137}Cs distribution in the
155 profiles located under cropland, as our model did not take tillage processes into account.
156
157 2.2 Modelling of radionuclide vertical distributions
158 The migration of fallout radionuclides in soils is often described using the diffusion-
159 convection equation (e.g. He and Walling 1997; Schuller et al. 1997):

160 $$\frac{\partial A}{\partial t} = \frac{\partial}{\partial z}\left(D_s \frac{\partial A}{\partial z} - v_s A\right) - \lambda A \quad (1)$$

161 With A- the total ^{137}Cs activity per volume of soil (Bq m^{-3}; obtained by multiplying the ^{137}Cs
162 activity in Bq kg^{-1} by the soil bulk density), z- the soil depth (m), t- the time (s), D_s- the
163 diffusion coefficients (m^2 s^{-1}), v_s- the convection velocity (m s^{-1}), λ- the radioactive decay
164 constant (s^{-1}). The diffusion coefficients D_s and the convection velocity v_s were considered as
165 spatially and temporally constant in this study. This is an over-simplification, as we know that
166 mixing processes and vertical transfers in soil may vary in both time and depth. However, we
167 considered that intensity of these processes remained constant during the last decades.
168 In the model, ^{137}C is given as a bulk concentration, hypothesising that ^{137}Cs is evenly
169 distributed within the soil mass of the considered layer. However, as ^{137}Cs is mainly deposited
170 as the result of wet fallout, its distribution is heterogeneous in soils and depends on soil
171 structure, macropore distribution and preferential flow (Bundt et al. 2000). Furthermore, it
172 evolves throughout time due to the occurrence of wetting/drying cycles and bioturbation, and
173 it depends on the soil moisture content at the time of deposition. Therefore, we acknowledge
174 that ^{137}Cs distribution in soils may be more complex than modelled in our study.
175
176 *2.2.1 Boundary conditions*
177 At the soil surface, we applied a boundary condition with a pulse-like input of radionuclides.
178 This pulse-like input was obtained by multiplying the annual fallout deposition $a_0(t')$ in Bq

179 m^{-2} of the considered year *t'* by a Dirac delta function $a(0, t') = a_0(t')\delta(t-t')$:

180 $$D_s \frac{\partial A(0,t')}{\partial z} = a_0(t')\delta(t-t') \quad (2)$$

181 Isotopes were delivered to the surface, at z=0, annually and input time-series were dealt as a
182 time-dependent boundary condition, i.e. $A(0, t') = A(0, t'-1)+a_0(t')\delta(t-t')$.
183 The annual global fallout input $a_{GF}(t')$ followed the distribution calculated by Cambray et al.
184 (1989) for various locations across the Northern Hemisphere, with a total fallout
185 accumulation of 3018 Bq m^{-2} before the Chernobyl accident in 1986. The global fallout was
186 latitude-dependent and it was reconstructed based on ^{90}Sr fallout recorded by UNSCEAR
187 (1982) in different latitudinal bands (Table 2). As the ^{137}Cs/^{90}Sr ratio was constant over time
188 (1.6 for global bomb fallout), ^{137}Cs fallout (Table 2) was deducted from ^{90}Sr measurements.
189 With respect to the total fallout accumulation of Cambray et al. (1989), we defined a weighted
190 factor maximum r_{th} as a function of the latitudinal position of the sampled site (Table 2).
191 Therefore global fallout contribution was determined as the product of the weighted factor r
192 and the annual global fallout a_{GF} (3). In the model, the weighted factor r was allowed to vary
193 between 0 and the maximal weighted factor r_{th} of the latitudinal band in which the sampling
194 site was located (Table 2). The factor r was considered as an unknown variable and was
195 estimated by the model for each profile. As ^{137}Cs input due to the Chernobyl accident (a_{Ch})
196 strongly varied across space, it was also considered as an unknown variable and was
197 estimated by the model. Hence, the temporal input variations were described as follows:

198 $$\begin{aligned} a(0,t') &= r a_{GF}(t')\delta(t-t') \quad 1954 \le t' < 1986 \\ a(0,t') &= a_{Ch}\delta(t-t') \quad t' = 1986 \end{aligned} \quad (3)$$

199 We applied as lower boundary condition (at 200 cm) an advective transport free of diffusion
200 in order to avoid spurious accumulation of radionuclides and not to influence the numerical
201 solution within the first 100 cm.

202

203 *2.2.2 Discretization and resolution of the equation*

204 We solved the differential Eq. (1) using upwind finite differences approximation for spatial
205 derivatives and semi-implicit Crank-Nicholson scheme as a time-solver. The obtained
206 algebraic system of equations was solved by Gaussian elimination. All the simulations started
207 in 1954 and finished on the sampling year. Time-step was equal to 0.01 year. The accuracy of
208 the numerical solution was verified by comparison with the analytical solution (4) obtained
209 with similar initial and boundary conditions:

$$A(z,t) = a_0 \left\{ \frac{1}{\sqrt{\pi D_s t}} \exp\left(-\frac{(z - v_s t)^2}{4 D_s t} \right) - \frac{v_s}{2D_s} \exp\left(\frac{v_s z}{D_s} \right) \operatorname{erfc}\left(\frac{v}{2}\sqrt{\frac{t}{D}} + \frac{z}{2\sqrt{Dt}} \right) \right\} \exp^{-\lambda t} \quad (4)$$

211 with a simple pulse-like input $(a_0(t)\delta(t))$ into a semi-infinite domain and a zero-concentration
212 when $z \to \infty$.

213

214 *2.2.3 Non-linear least square minimization procedure*

215 The unknown parameters (D_s, v_s, r, a_{Ch}) and their standard deviations were determined with a
216 non-linear least-square minimization procedure based on the Levenberg-Marquardt algorithm
217 included in Python *lmfit* package. The minimized value for each measurement A_m (in Bq cm^{-3})
218 was calculated in an integral form, which provided a way to take different sampling intervals
219 into account (Bossew and Kirchner, 2004):

$$\operatorname{argmin} = \left(A_m (z_2 - z_1) - \int_{z_1}^{z_2} A(z,t)\,dz \right)^2 \quad (5)$$

221 In order to estimate the performance of the fitting procedure, we calculated residual sum of
222 squares (*RSS*) for N sampled layers and modelling efficiency (*EF*):

$$RSS = \sum_{i=0}^{N} \left(A_m(i)(z_{i2} - z_{i1}) - \int_{z_{i1}}^{z_{i2}} A(z,t)\,dz \right)^2 \quad (6)$$

$$EF = 1 - \frac{\sum_{i=0}^{N}\left(\int_{z_{i1}}^{z_{i2}} A(z,t)dz - A_m(i)(z_{i2}-z_{i1})\right)^2}{\sum_{i=0}^{N}\left(A_m(i)(z_{i2}-z_{i1}) - \frac{1}{N}\sum_{i=0}^{N}A_m(i)\right)^2} \quad (7)$$

The first simulation was run to fit all 4 parameters (D_s, v_s, r, a_{Ch}). If the resulting model parameters remained in the range of possible values ($0 < r \leq r_{th}$, $0 \leq a_{Ch}$), the simulation was retained as the best fit. Otherwise, we added the following assumptions: $a_{Ch} = 0$ if the sampling site was located in a region spared by Chernobyl deposits and $ra_{GF} = 4\,527$ Bq m^{-2} (the maximum global fallout input) if the model attributed larger global fallout input than expected, which was often the case for the sites characterised by high levels of Chernobyl contamination. All sites affected by soil erosion or soil accumulation were excluded from the database for further analysis, and these processes were therefore not simulated by the model.

3 Results and discussion

3.1 Soil bulk density within the uppermost 20 centimetres of the soil: evolution and estimation

Bulk densities reported in the literature for 13 soil profiles ranged from 0.6 to 1.41 g cm^{-3} at 5-cm-depth and from 0.9 to 1.47 g cm^{-3} at 20-cm-depth. The mean bulk density of these 13 soil profiles evolved with depth following a logarithmic function (Fig. 1a; eq. 8):

$$\rho(z) = C_1 \ln(z) + C_2 \quad (8)$$

with depth z expressed in cm. For the considered soil profiles, C_1 was equal to 0.1636 and C_2 to 0.7329 (R^2=0.94).

We considered a comparable evolution of the bulk density in depth for the other profiles, with the same C_1 value, whereas C_2 was estimated in order to fit the total ^{137}Cs inventory (I) considering the depth evolution of the activities of ^{137}Cs in Bq kg^{-1}, using the minimization equation (9):

$$\arg\min = \left(\sum_{i=0}^{N} \left(\left(C_1 \ln\left(\frac{z_{i2} + z_{i1}}{2} \right) + C_2 \right) A_s(i) (z_{i2} - z_{i1}) \right) - I \right)^2 \quad (9)$$

In order to check the accuracy of the obtained predictive model, bulk densities were estimated for the soil profiles for which these data were available (Fig. 1b). We obtained a reasonable estimation of the bulk density in samples close to the surface, but the density was underestimated by the model below 10 cm depth. However, as only a small proportion of the ^{137}Cs was located at this depth, the impact of bulk density underestimation on ^{137}Cs vertical distribution was considered to be negligible.

The model was applied to the 48 soil profiles for which bulk density data were not available (Electronic Annex A). C_2 varied between 0.37 and 2.53. Eighty percent of the mean bulk density of the 0-20 cm layer - estimated by the predictive model - ranged from 0.94 to 1.66 g cm^{-3}, with a median value of 1.22 g cm^{-3}. The estimated soil bulk densities were considered as irrelevant in 5 profiles compared to the values classically found in soils. In addition, negative values were obtained in 4 profiles. They were therefore not considered in further analysis.

3.2 Cs-137 distributions in soils

The recorded ^{137}Cs inventories (decay-corrected for 2013) ranged from 697 Bq m^{-2} to 107 200 Bq m^{-2}. The highest inventories were measured in soils collected in the areas severely contaminated by Chernobyl fallout in central Europe and Sweden as documented in the atlas of Chernobyl contamination (De Cort et al. 1998). The depth of the maximum concentration (z_{maxC}) ranged between 0 and 12 cm (with a median value of 2 cm) and the maximal penetration depth (*i.e.* with a ^{137}Cs concentration higher than or equal to 0.001 Bq cm^{-3}) ranged between 12 cm and 60 cm. Width of the peak (estimated as Half Width at Half Maximum (*HWHM*)) ranged between 1.25 and 13.7 cm (median of 5 cm). We could not identify any clear relationship between the soil groups and the depth of maximum

272 concentration, maximum depth or width of the peak.

273 Based on the depth of maximum ^{137}Cs concentration, the width of peak and the shape of
274 radiocesium profile, we determined 7 classes of depth distribution profiles (Fig. 2):

275 1- Continuous decrease in the concentrations with depth ($z_{maxC} = 0$ cm and $HWHM \leq 5$ cm -
276 13 profiles);

277 2- Half bell-shaped curve with maximum concentration at the soil surface. The concentrations
278 decrease with depth following a Gaussian-like shape ($z_{maxC} = 0$ cm and $HWHM > 5$ cm - 10
279 profiles);

280 3- Narrow hump-shaped curve at shallow depth with a maximum concentration comprised
281 between 0 and 2 cm depth ($0 < z_{maxC} \leq 2$ cm and $HWHM \leq 5$ cm - 25 profiles);

282 4- Wide hump-shaped curve shape at shallow depth with a maximum concentration within the
283 0-2 cm depth interval ($0 < z_{maxC} \leq 2$ cm and $HWHM > 5$ cm - 13 profiles);

284 5- Narrow hump-shaped curve with maximum concentration deeper than 2 cm ($z_{maxC} > 2$ cm
285 and $HWHM \leq 5$ cm - 12 profiles);

286 6- Wide hump-shaped curve with maximum concentration deeper than 2 cm ($z_{maxC} > 2$ cm and
287 $HWHM > 5$ cm - 18 profiles);

288 7- Constant isotopic profile concentration over depth (4 profiles).

289

290 As ^{137}Cs fate in the soil depends on the soil characteristics and processes, ^{137}Cs depth
291 distribution should be a function of the soil groups. It was however not the case (Table 3).
292 Other factors may influence the distribution profile such as the duration since the ^{137}Cs input
293 or the climate conditions.

294 VandenBygaart et al. (1998), Tyler et al. (2001), Bunzl (2002), Kaste et al. (2007), Elshamy
295 et al. (2007), Ireson and Butler (2009), Jarvis et al. (2010) and Matisoff et al. (2011)
296 demonstrated the impact of bioturbation on radionuclide redistribution in soil profiles. The

297 importance of bioturbation may be estimated from the width of the peak: highly active
298 bioturbation leads to wider shaped curves. We would thus expect stronger bioturbation in the
299 profile types 2, 4, 6 than in profile types 1, 3, 5. As bioturbation depends on the mean annual
300 temperature, it should be more intense under warm climates than under cold or dry climates.
301 Table 4 shows the climate distribution for the different profile types as it was determined
302 from the location of the sampling site and the climate classification according to Kottek et al.
303 (2006). However, depth distribution profiles 2, 4, 6 were not more frequent under warm
304 temperate and humid climates (C classes of Köppen's climate classification, 32 profiles out of
305 69), than under dry or cold climates (B and D classes of Köppen's climate classification; 8 out
306 of 20). Land use or cover may also impact the ^{137}Cs distribution. Most of the type-1
307 distribution profiles corresponding to Cambisols were collected under forests whereas
308 peatlands corresponded to type 5 (n = 2). All the cultivated plots were attributed to type 7
309 (n = 4).
310 The soil profiles were sampled between 1992 and 2007. The classification of different soils of
311 a same soil group according to different depth-profile types may be explained by the temporal
312 evolution of the initial profile. Indeed, after ^{137}Cs inputs, the peak progressively migrates in
313 depth, and its distribution profile will widen with time depending on the turbation rate. This
314 evolution will nevertheless depend on the time elapsed after the main ^{137}Cs input that may
315 either be due to the bomb tests or to the Chernobyl accident depending on the site. This
316 probably explains why we could not find any relationship between ^{137}Cs depth profiles and
317 the sampling dates. In addition, for similar sampling dates, classification according to
318 different profile shapes may originate from differences in values of diffusion coefficient (D_s
319 in cm^2 yr^{-1}) and convection velocity (v_s in cm yr^{-1}): profile type 1 being obtained for $D_s > 0$
320 and $v_s \approx 0$; profile type 2 for $D_s >> 0$ and $v_s \approx 0$; profile type 3 for $D_s > 0$ and $v_s > 0$; profile
321 type 4 for $D_s >> 0$ and $v_s > 0$; profile type 5 for $D_s > 0$ and $v_s >> 0$; and profile type 6 for D_s

322 >> 0 and v_s >> 0. The profiles belonging to class 7 result either from a disturbance or from a
323 mixing of the entire profile that may have been achieved by agricultural practices such as
324 tillage.
325 As a conclusion, the ^{137}Cs profile type is a complex result of the variations in soil processes
326 affecting the diffusion and convection transport and resulting in contrasted temporal
327 evolutions.
328
329 3.3 Diffusion and convection in soils
330 *3.3.1 Overall quality of the simulation results*
331 We have simulated the evolution of 71 profiles out of the 99 profiles compiled in the database
332 (detailed results are provided in the Electronic Annex A and B). We have excluded 4
333 cultivated profiles, 4 profiles with thick organic horizons containing more than 30 % of the
334 total ^{137}Cs inventory, 4 profiles with unrealistic bulk density values and 16 profiles with only
335 3 measurements per profile, which was insufficient for optimizing the 4 required parameters.
336 Overall, modelling efficiency (*EF*) reached a mean of 0.89 ± 0.20, and a median of 0.96
337 (max(*EF*) = 1), which is fairly good. The comparison between simulated and observed ^{137}Cs
338 concentrations in all profiles showed a reasonable agreement with some underestimation at
339 low concentrations (Fig. 3). Scaled residuals as a function of ^{137}Cs concentrations were
340 normally distributed. However, when considered as a function of depth (Fig. 4), residuals
341 were normally distributed and centred at zero in the first 13 cm only. They shifted towards
342 positive values below 13 cm and they were all positive below 30 cm. This demonstrates that
343 the model underestimated ^{137}Cs concentrations in most samples collected below 13 cm and
344 that it underestimated all values below 30 cm.
345 Finally, v_s was null for 23 profiles. These profiles exhibited large standard deviation values
346 for all parameters. The model could therefore not differentiate the inputs due to global fallout
347 from those due to the Chernobyl accident, and the estimation of D_s coefficient satisfied a wide

348 range of values.

349

350 *3.3.2 Estimation of global fallout*

351 We have compared the global fallout ra_{GF} values optimized by our model to the range of
352 fallout estimations provided by UNSCEAR (1982) for different latitudes (Table 2). In 59 % of
353 the cases, the modelled global fallout values were equivalent to the values estimated by
354 UNSCEAR (1982), but they were lower in the remaining 41% of the sites. However, the
355 values estimated by UNSCEAR (1982) may have been affected by other local factors such as
356 rainfall. As an example, Cambray et al. (1989) provided lower values of global fallout
357 compared to UNSCEAR (1982) for regions located in the 40-50°N band. Furthermore,
358 extremely low values of global fallout were obtained for the sites located in arid regions in
359 Syria, reaching even zero at several places (4 sites). The lower fallout obtained in this region
360 compared to those estimated by UNSCEAR (1982) probably reflects the absence of
361 precipitations (Aoyama et al. 2006).
362 The occurrence of soil erosion between the end of 1960s and Chernobyl accident may also
363 explain the lower values of global fallout obtained for several profiles. However, no data
364 (such as the history of land use or cover of the corresponding sites) were available to verify
365 this hypothesis. In addition, erosion was probably very limited at these sites, since they were
366 generally covered by vegetation (forest, grassland) and were therefore considered as
367 undisturbed.
368 For three Swedish sites located between 62 and 64°N, the use of the global fallout of the 50-
369 60°N band with higher fallout rates improved the modelling efficiency compared to the one
370 obtained when taking values of the 60-70° band. Similarly, Sigurgeirsson et al. (2005)
371 reported that ^{137}Cs deposition was underestimated for 60-70° N band by UNSCEAR (1982) in
372 Icelandic soils. We observe the same phenomena for Chinese sites at 29°N, showing that the

373 latitude parallels defining the limit between two bands should be rather considered as buffer
374 (transition?) zones.
375 Overall, differences between observed and simulated global fallout may be explained by: (i),
376 a virtual absence of fallout because of the lack of precipitation in arid regions (as it was
377 probably the case in Syria); (ii), the possible occurrence of soil erosion between the end of
378 1960s and Chernobyl accident.
379
380 *3.3.3 Possible mechanisms behind D and v*
381 Diffusion coefficient is widely used to estimate bioturbation in the literature (e.g. Elzein and
382 Balesdent 1995; Schiffers et al. 2011). Bioturbation in soil is due to the activity of micro- and
383 macro-organisms. Under temperate climates, it is mainly controlled by earthworm activity
384 (Wilkinson et al. 2009). However, diffusion coefficient only represents a local mixing,
385 whereas a non-negligible part of bioturbation may be due to non-local feeder earthworm
386 species (Jarvis et al. 2010; Schiffers et al. 2011). As the diffusion coefficient is unable to
387 simulate this non-local behaviour, alternative models were developed (Müller-Lemans and
388 van Drop, 1996; Schiffers et al. 2011). A non-local mixing term was integrated into the
389 general diffusion-convection equation (Jarvis et al. 2010), which improved the simulations of
390 deep penetration of ^{137}Cs. The transfer function describing the behaviour of non-local feeders
391 requires the implementation of other parameters (*i.e.* ingestion rate of non-local feeders, depth
392 of ingestion), which were calibrated by Jarvis et al. (2010) for their field-site based on an
393 ecological study of anecic and endogeic earthworm species (i.e., classical non-local feeders in
394 temperate soils). As such data were not available for the study sites, we could not model the
395 behaviour of non-local feeders. However, Jarvis et al. (2010) showed that estimating
396 bioturbation with a diffusion coefficient fits reasonably well with ^{137}Cs profiles, although it
397 underestimates concentrations at depth.

398 The simulated diffusion coefficients D_s ranged from 0.02 to 4.44 $cm^2\ yr^{-1}$ (median of 0.64 cm^2
399 yr^{-1}). Among the profiles compiled in our database, modelling had already been conducted on
400 35 soils using different methods for solving the diffusion-convection equation (Szerbin et al.
401 1999; Krstic et al. 2004; Schimmack and Márquez 2006; Zhang et al. 2008; Legarda et al.
402 2011). These studies obtained a median D_s value of 0.53 $cm^2\ yr^-1$, which is slightly different
403 from our findings. However, this discrepancy may be explained by the inclusion of ca. 40
404 additional profiles in our study, which may have enlarged the range of D_s values in soils.
405 These D_s values were the highest for depth-distribution type 4 (mean of 1.4 $cm^2\ yr^{-1}$). Then,
406 they were higher for depth distribution types 2, 3, and 6 (mean ranging from 0.8 to 1.3 $cm^2\ yr^-$
407 ^{1}) than for depth distribution types 1 and 5 (mean of 0.5 $cm^2\ yr^{-1}$; ANOVA with a Fisher test
408 at 5 % level of confidence).
409 We could not observe any significant difference in D_s values as a function of land use or
410 cover, the time elapsed after the main ^{137}Cs input, soil group or the climate type.
411 One of the difficulties associated with our approach is that D_s may account for both a
412 diffusion process and a dispersion of the convection velocities when the convection operates.
413 Therefore, a correlation between both parameters may indicate that D_s is not exclusively
414 linked to bioturbation but that it is also affected by convection processes. However, we did
415 not observe any correlation between D_s and either the precipitation or v_s when considering the
416 entire set of profiles. When the different soil groups were considered separately (Fig. 5), D_s
417 remained independent from v_s in Luvisols and Regosols, whereas in Yermosols, a positive
418 linear relationship was observed between D_s and v_s ($D_s = 4.13v_s + 0.08$, $R^2 = 0.84$, n = 8). This
419 relationship suggested that an important dispersive effect exists in Yermosols with increasing
420 convection velocity. The relatively high D_s values observed in this soil group under a dry
421 climate are therefore likely due to the convection process occurring in these soils and not to
422 bioturbation, which is probably low under dry climate conditions. In Cambisols, i.e. the most

423 documented soil group (n = 19), three trends between D_s and v_s were observed: a variable
424 diffusion at zero-velocity, a slight dispersion with increasing v_s and a high dispersion.
425 Although they were not significantly different, D_s values lower than 0.2 $cm^2\ yr^{-1}$ were
426 generally found either in the soils experiencing podzolization or gleization (Spodic Dystric
427 Cambisols, Hypogleyic Cambisols, Podzols, Gleyic Phaeozems) or in soils collected in
428 Northern regions (latitude > 60°N with the exception of a Histosol profile sampled in Hille,
429 Sweden). Soils of the first group were acidic and thus unfavourable to bioturbing organisms,
430 whereas in the second group bioturbation was limited because of the cold climate conditions.
431 In Cambisols and Regosols, D_s increased with soil pH (R of 0.50 for n = 13 in Cambisol). For
432 the other soil groups, the soil pH data were too scarce to draw any conclusion. Finally, the
433 high D_s values obtained for Chernozems and Vertisols may be due to the occurrence of
434 specific pedological processes in these soils (organic matter diffusion and turbation via
435 shrinking and swelling, respectively), rather than to bioturbation (Table 5).
436 The v_s coefficient can be considered as representative of the transfer of ^{137}Cs that was either
437 adsorbed on the clay surface - and that may therefore reflect clay translocation-, or that was
438 dissolved in organic rich soils. In this study, v_s ranged from 0 to 0.74 cm yr^{-1} (median of 0.1
439 cm yr^{-1}). These values were of the same order of magnitude as those obtained for the 35
440 profiles that were previously modelled in the literature (Szerbin et al. 1999; Krstic et al. 2004;
441 Schimmack and Márquez 2006; Zhang et al. 2008; Legarda et al. 2011). The v_s values ranked
442 as follows from the highest to the lowest: types 5 and 6 (mean ranging from 0.27 to 0.35 cm
443 yr^{-1}) > type 3 and 4 (mean ranging from 0.13 to 0.15 cm yr^{-1}) > type 1 and 2 (mean ranging
444 from 0 to 0.01 cm yr^{-1}) (ANOVA with a Fisher test at 5 % level of confidence). Zero-velocity
445 occurred in 23 profiles corresponding to different soil groups: Acrisols (n=1), Cambisols
446 (n=7), Fluvisols (n=2), Histosols (n=3), Leptosols (n=1), Regosols (n=2), Solonetz (n=2),
447 Vertisols (n=2) and Yermosols (n=3). We could not identify the key parameter responsible for

448 these zero-velocities. Significant differences in v_s were observed under various land uses and
449 covers, with the highest v_s values found under peatland (0.38 cm yr^{-1}, n=2) and the lowest
450 under forests (0.07 cm yr^{-1}, n=6), soils located under grassland being associated with
451 intermediary v_s values (0.14 cm yr^{-1}, n=63).
452 Several authors found that migration velocity of ^{137}Cs decreased with time after the
453 radionuclide input (Alexakhin and Krouglov, 2001). To test the impact of this parameter, we
454 calculated the time elapsed since the main ^{137}Cs input considering the simulated respective
455 contributions of global fallout and Chernobyl accident (all values were decay-corrected to the
456 sampling date). The simulated v_s values for the entire set of profiles decreased with time (T)
457 after the main ^{137}Cs input (R=-0.32, n=71; Fig. 6).
458 When considering the different soil groups, velocities were independent of the time after the
459 main input in Vertisols, Solonetzs, Luvisols, Fluvisols and Cambisol. For the two first soil
460 groups, v_s were systematically lower than 0.11 cm yr^{-1}, whereas in Luvisols, velocities were
461 relatively high (0.22±0.06 cm yr^{-1}). They ranged from 0 to 0.43 yr cm^{-1} in Fluvisols and
462 Cambisols. In Leptosols, Podzols, Regosols and Yermosols, the velocities decreased with
463 time, whereas they increased in Histosols.
464 In addition, Histosols showed two populations of profiles: profiles with a high D_s value
465 (> 1.5 cm^2 yr^{-1}) and a v_s close to 0 cm yr^{-1} or profiles with the highest v_s values (v_s > 0.2 cm yr^{-1} with D_s < 0.2 cm^2 yr^{-1}). The highest v_s values were simulated in peatland profiles, whereas
467 the lowest velocities were obtained for Histosols under forest or grassland. In addition v_s
468 values increased with time. As discussed in the introduction, transport of ^{137}Cs in dissolved
469 form can partially explain the simulated v_s values in Histosols that contain more than 20% of
470 organic matter. Their relatively lower value when Histosol were collected under grassland or
471 forest is probably due to a partial absorption of the soluble fraction of ^{137}Cs by the vegetation.
472 In the case of Luvisols, Acrisols, Solonetz and Cambisols, the obtained v_s values may reflect

473 the occurrence of clay translocation, as clay translocation is a major pedogenic process in
474 Luvisols, Acrisols and Solonetz, and secondary pedogenic process in Cambisols (FAO 1998;
475 Bockheim and Gennadiyev 2000). The significantly higher v_s values obtained for Luvisols
476 (ANOVA with a Fisher test at 5 % level of confidence, Table 5) are consistent with the
477 occurrence of clay translocation in this soil group. Clay translocation may also explain some
478 of the few high v_s values found in Cambisols. However, some profiles corresponding to these
479 soil groups have a v_s value equal to 0 cm yr^{-1} (Acrisols for example) or positive but extremely
480 low values (Solonetz with a mean v_s of 0.03 cm yr^{-1}). In these soils, clay translocation might
481 not have been active since the beginning of the ^{137}Cs release into the atmosphere. This finding
482 is consistent with the fact that this process is only active in soils where pH ranges from 5 to
483 6.5 (Quénard et al. 2011), except in sodic soils (Solonetz for example).
484
485 *3.3.4 Global penetration velocity of caesium-137*
486 Soils compiled in the database were submitted to different inputs of ^{137}Cs and were sampled
487 at various dates. As mentioned above, these parameters control the actual depth of
488 penetration. We modelled D_s and v_s that are responsible for the penetration of caesium in the
489 soils, but these parameters did not provide a direct picture of the penetration velocity of
490 caesium in the soil. To obtain it, we calculated the mean depth reached by ^{137}Cs after 25 years
491 of migration, considering that ^{137}Cs was instantaneously injected into the soil as a Dirac
492 distribution representing a 'spike' of concentrated ^{137}Cs (Table 5). Mean penetration velocity
493 of ^{137}Cs over 25 years varied between 0.05 and 0.76 cm yr^{-1} (median of 0.28 cm yr^{-1}). When
494 calculated over 50 years, these values decreased by about 20 % in average because of
495 diffusive processes and ranged from 0.04 to 0.71 cm yr^{-1} (median of 0.21 cm yr^{-1}).
496
497 *3.3.5 Caesium-137 content at depth below 13 cm*

498 As mentioned before, the distribution of scaled residuals suggested that the model
499 underestimated the deep penetration of ^{137}Cs below 13 cm. We therefore estimated the
500 unmodelled Cs inventory and quantified its migration rate. The proportion of the inventory
501 underestimated by the model below 13 cm ranged between -3.8 and 37.2 %, with a median
502 value of 1.9 %. The mean transfer rate below 13 cm was then calculated by dividing the
503 underestimated fraction by the time after the main ^{137}Cs input. It ranged from 7.5 to 44.1
504 years (median of 20.1 years) and the obtained rate of transfer below 13 cm varied from 0 to
505 0.02 yr^{-1} (median of 0.001 yr^{-1}). As discussed above, this transfer in depth could be due to the
506 behaviour of non-local feeders. Matisoff et al. (2011) estimated that the feeding rate of non-
507 local feeders ranged from 0.002 to 0.02 yr^{-1} depending on the soil group. As our results are of
508 the same order of magnitude, this suggests that non-local feeders could be responsible for
509 these deep transfers.
510
511 *3.3.6 Approximations in the model: implications for estimating solid matter transfers*
512 Initial distribution of radionuclides was modelled as an injection at the surface (z=0), which is
513 an over-simplification as ^{137}Cs wet deposits are inherently heterogeneous. Cs-137 is most
514 likely sorbed in soil macropores, and sorbing zones are affected by preferential flow (Bundt et
515 al. 2000), which depends itself on soil structure and moisture. Prediction of initial ^{137}Cs
516 distribution is therefore case-dependent and as such, it is difficult to reproduce in a general
517 modelling approach.
518 Furthermore, in our modelling approach, we considered that the diffusion and convection
519 velocity coefficients were constant in time and depth. However, some authors predicted a
520 decrease in migration velocities with time (Alexakhin and Krouglov 2001). Nevertheless, as
521 outlined by Kirchner (1998), this apparent decrease simulated by compartment models may
522 be explained by the occurrence of the diffusive process itself. The heterogeneous distribution

523 of ^{137}Cs can also be a cause of this decrease: ^{137}Cs was likely initially located on the surface
524 of macropores and aggregates and it was then progressively incorporated within the soil
525 matrix and become therefore less mobile. Nevertheless, it has been shown that preferential
526 flow paths (and thus the soil structure) may remain stable for more than 40 years in soils
527 (Bundt et al. 2000). Moreover, pedogenic processes affecting the vertical solid matter
528 transfers such as bioturbation were recognized to be depth-depend (Müller-Lemans and Van
529 Dorp 1996). Similarly, integrating non-local feeders modelling as in Jarvis et al. (2010) has a
530 direct influence on the soil displacement rate (corresponding to v_s in our study), which
531 decreased linearly with depth in the feeding zone. Therefore, we expect that the inclusion of
532 depth-variable coefficients in the model may improve simulations of ^{137}Cs distributions at
533 depths < 13 cm. However, including spatially variable coefficients in the model would require
534 the inclusion of new parameters (at least 2 additional factors to account for exponentially
535 decreasing D_s and v_s), the improvement of the database or the collection of additional samples
536 and measurements in the field.
537
538 **4 Conclusions**
539 The modelling approach proposed in this study provides an original basis for comparing ^{137}Cs
540 depth migration in different soil groups. However, no difference of global ^{137}Cs penetration
541 velocities was observed among soil groups. It ranged from 0.05 to 0.76 cm yr^{-1} (median of
542 0.28 cm yr^{-1}), with a significantly lower velocity for soil groups poorly evolved (Regosol),
543 and a significantly higher for soils rich in organic matter (Histosols). The model
544 underestimated this velocity under a 13-cm depth. In the future, the model could be improved
545 by introducing a non-local feeder term or by allowing D_s and v_s values to vary with soil depth
546 in the diffusion-convection equation.
547 D_s and v_s values explained the depth profile of ^{137}Cs in soils and were shown to partly reflect

548 the occurrence of turbation including bioturbation for D_s and clay translocation for v_s, except
549 in Histosols where the transfer of ^{137}Cs in dissolved form was very likely. D_s values ranged
550 from 0.02 to 4.44 $cm^2\ yr^{-1}$ (median of 0.64 $cm^2\ yr^{-1}$) and v_s varied from 0 to 0.74 $cm\ yr^{-1}$
551 (median of 0.1 $cm\ yr^{-1}$).
552 Due to the limited number of documented profiles per soil group and other potential sources
553 of variability that could not be documented (climate, land use or cover, pH), it was not
554 possible to attribute precisely D_s and v_s variations to the occurrence of different soil processes.
555 However, clear trends were observed for certain soil groups. Lower D_s values were simulated
556 in acidic soils or under cold climate conditions, and they likely reflected the lower-intensity
557 bioturbation prevailing under those pedoclimatic conditions. In addition, high v_s values were
558 simulated in soils submitted to clay translocation (notably Luvisols). A relationship was also
559 derived between v_s and certain land uses or covers. In this context, our results showed that
560 modelling ^{137}Cs depth-profile with a diffusion-convection equation allowed estimating the
561 bioturbation and clay translocation velocity in a certain number of soil groups. Although the
562 occurrence of these soil processes is well known in most soils, they have been rarely
563 quantified. Still, this quantification is crucial as these processes partially control the
564 development of soil surface characteristics and several soil services such as plant nutrition,
565 organic carbon storage or pollutant fixation. In the future, to overcome the limitations
566 associated with the modelling of diffusion-convection parameters based on ^{137}Cs
567 measurements, we suggest to conduct a multi-isotopic characterisation of different types of
568 soil profiles in order to quantify the relative contribution of the different processes responsible
569 for vertical solid matter transfer.
570
571 **Acknowledgments -** The authors are grateful to Dr. Jérôme Balesdent for his helpful advises,
572 as well to Dr. Frédéric Golay, Dr. Cédric Galusinski and Dr. Gloria Faccanoni for their help

573 with model simulations. We thank the French Research Agency (ANR) that funded the
574 Agriped project (ANR 10 Blanc 605). M. Jagercikova received a PhD fellowship from the
575 French National Institute of Agronomy (INRA). We are also grateful to Dr. Luise Giani, Dr.
576 Gwen Milton, Dr. Concepción Olondo Castro and Dr. Klas Rosén for kindly providing their
577 soil datasets and additional information regarding their studies.
578

579 **References**

580 AIEA (2010) Handbook of Parameter Values for the Prediction of Radionuclide Transfer in
581 Terrestrial and Freshwater Environments. Technical Reports SeriEs No. 472.
582 International Atomic Energy Agency
583 Al-Masri M (2006) Vertical distribution and inventories of Cs-137 in the Syrian soils of the
584 eastern Mediterranean region. J Environ Radioact 86:187-198
585 Alexakhin RM, Krouglov SV (2001) Soil as the main compartment for radioactive substances
586 in terrestrial ecosystems. In: Bréchignac F, Howard BJ (eds) Radioactive pollutants.
587 Impact on the environment, EDP Sciences, Les Ulis, France, pp 149-174
588 Aoyama M, Hirose K, Igarashi Y (2006) Re-construction and updating our understanding on
589 the global weapons test 137Cs fallout. J Environ Monit 8:431-438
590 Ben Slimane A, Raclot D, Evrard O, Sanaa M, Lefèvre I, Ahmadi M, Tounsi M, Rumpel C,
591 Ben Mammou A, Le Bissonnais Y (2013) Fingerprinting sediment sources in the
592 outlet reservoir of a hilly cultivated catchment of Tunisia. J Soils Sediments 13:801-
593 815
594 Bockheim J, Gennadiyev A (2000) The role of soil-forming processes in the definition of taxa
595 in Soil Taxonomy and the World Soil Reference Base. Geoderma 95:53-72
596 Bossew P, Kirchner G (2004) Modelling the vertical distribution of radionuclides in soil. Part
597 1: the convection-dispersion equation revisited. J Environ Radioact 73:127-150

598 Bunzl K (2002) Transport of fallout radiocesium in the soil by bioturbation: a random walk
599 model and application to a forest soil with a high abundance of earthworms. Sci Total
600 Environ 293:191–200
601 Bunzl K, Kracke W, Schimmack W, Zelles L (1998) Forms of fallout Cs-137 and Pu239+240
602 in successive horizons of a forest soil. J Environ Radioact 39:55-68
603 Bunzl K, Schimmack W, Zelles L, Albers B (2000) Spatial variability of the
604 vertical migration of fallout Cs-137 in the soil of a pasture, and consequences for long-
605 term predictions. Radiat Environ Biophys 39:197-205
606 Bundt M, Albrecht A, Froidevaux P, Blaser P, Flühler H (2000) Impact of preferential flow
607 on radionuclide distribution in soil. Environ Sci Tech 34:3895-3899
608 Cambray RS, Playford K, Lewis G, Carpenter R (1989) Radioactive fallout in air and rain:
609 results to the end of 1988. Environmental and Medical Sciences Division, United
610 Kingdom Atomic Energy Authority
611 Chartin C, Evrard O, Onda Y, Patin J, Lefèvre I, Ayrault S, Lepage H, Bonté P (2013)
612 Tracking the early dispersion of contaminated sediment along rivers draining the
613 Fukushima radioactive pollution plume. Anthropocene 1: 23-34
614 Cremers A, Elsen A, Depreter P, Maes A (1988) Quantitative-analysis of radiocesium
615 retention in soils. Nature 335:247-249
616 De Cort M, Dubois G, Fridman SD, Germenchuk MG, Izrael YA, Janssens A, Jones AR,
617 Kelly GN, Kvasnikova EV, Matveenko II, Nazarov IM, Pokumeiko YM, Sitak VA,
618 Stukin ED, Tabachnyi LY, Tsaturov YS, Avdyushin SI (1996) Atlas of caesium
619 deposition on Europe after the Chernobyl accident. EUR Report 16733, EC, Office for
620 Official Publications of the European Communities, Luxembourg
621 De Vos B, Van Meirvenne M, Quataert P, Deckers J, Muys B (2005) Predictive quality of
622 pedotransfer functions for estimating bulk density of forest soils. Soil Sci Soc Am J

69:500-510

Elshamy M, Mathias S, Butler A (2007) Demonstration of radionuclide transport modelling under field conditions: 50-year simulation of caesium migration insoil. Tech. Rep. Imperial/ NRP_016, United Kingdom Nirex Limited

Elzein A, Balesdent J (1995) Mechanistic simulation of vertical distribution of carbon concentrations and residence times in soils. Soil Sci Soc Am J 59:1328-1335

FAO (1998) World reference base for soil resources. World Soil Resources Rep. 84, Rome

Gallagher D, McGee E, Mitchell P (2001) A recent history of C-14, Cs-137, Pb-210, and Am-241 accumulation at two Irish peat bog sites: An east versus west coast comparison. Radiocarbon 43:517-525

Gil-Garcia C, Rigol A, Vidal M (2009) New best estimates for radionuclide solid liquid distribution coefficients in soils. Part 1: radiostrontium and radiocaesium. J Environ Radioact 100:690-696

He Q, Walling D (1997) The distribution of fallout Cs-137 and Pb-210 in undisturbed and cultivated soils. App Radiat Isot 48:677-690

Ireson M, Butler A (2009) A review of soil bioturbation and soil development. Tech. Rep. Imperial/NRP_018, United Kingdom Nirex Limited

Isaksson M, Erlandsson B, Mattsson S (2001) A 10-year study of the Cs-137 distribution in soil and a comparison of Cs soil inventory with precipitation-determined deposition. J Environ Radioact 55:47-59

Jarvis NJ, Taylor A, Larsbo M, Etana A, Rosen K (2010) Modelling the effects of bioturbation on the re-distribution of 137Cs in an undisturbed grassland soil. Eur J Soil Sci 61:24-34

Karadeniz O, Yaprak G (2008) Geographical and vertical distribution of radiocesium levels in coniferous forest soils in Izmir. J Radioanal Nucl Chem 277:567-577

Kaste JM, Heimsath AM, Bostick, BC (2007) Short-term soil mixing quantified with fallout radionuclides. Geology 35:243-246

Kirchner G (1998) Applicability of compartmental models for simulating the transport of radionuclides in soil. J Environ Radioact 38:339-352

Konoplev A, Bulgakov A, Popov V, Hilton J, Comans R (1996) Long-term investigation of Cs-137 fixation by soils. Radiation Protection Dosimetry 64:15-18

Korsakissok I, Mathieu A, Didier D (2013) Atmospheric dispersion and ground deposition induced by the fukushima nuclear power plant accident: a local-scale simulation and sensitivity study. Atmos Environ 70:267-279

Kottek M, Grieser J, Beck C, Rudolf B, Rubel F (2006) World map of the Koppen Geiger climate classification updated. Meteorologische Zeitschrift 15(3):259-263

Krstic D, Nikezic D, Stevanovic N, Jelic M (2004) Vertical profile of ^{137}Cs in soil. App Radiat Isot 61:1487-1492

Kruse-Irmer S, Giani L (2003) Vertical distribution and bioavailability of Cs-137 in organic and mineral soils. J Plant Nutr Soil Sci 166:635-641

Kruyts N, Delvaux B (2002) Soil organic horizons as a major source for radiocesium biorecycling in forest ecosystems. J Environ Radioact 58:175-190

Legarda F, Romero LM, Herranz M, Barrera M, Idoeta R, Valino F, Olondo C, Caro A (2011) Inventory and vertical migration of Cs-137 in Spanish mainland soils. J Environ Radioact 102:589-597

Lepage H, Evrard O, Onda Y, Patin J, Chartin C, Lefèvre I, Bonté P, Ayrault S (2014) Environmental mobility of ^{110m}Ag: lessons learnt from Fukushima accident (Japan) and potential use for tracking the dispersion of contamination within coastal catchments. J Environ Radioactiv 130:44-55

Mabit L, Benmansour M, Walling DE (2008) Comparative advantages and limitations of the

673 fallout radionuclides Cs-137, Pb-210(ex) and Be-7 for assessing soil erosion and
674 sedimentation. J Environ Radioactiv 99:1799-1807
675 Matisoff G, Ketterer ME, Rosen K, Mietelski JW, Vitko LF, Persson H, Lokas E (2011)
676 Downward migration of Chernobyl-derived radionuclides in soils in Poland and
677 Sweden. Appl Geochem 26:105-115
678 Milton G, Kramer S, Watson W, Kotzer T (2001) Qualitative estimates of soil disturbance in
679 the vicinity of CANDU stations, utilizing measurements of Cs-137 and Pb- 210 in soil
680 cores. J Environ Radioact 55:195-205
681 Müller-Lemans H, van Dorp F (1996) Bioturbation as a mechanism for radionuclide transport
682 in soil: Relevance of earthworms. J Environ Radioact 31:7-20
683 Noordijk H, Van Bergeijk KE, Lembrechts J, Frissel MJ (1992) Impact of ageing and weather
684 conditions on soil-to-plant transfer of radiocesium and radiostrontium. J Environ
685 Radioact 15:277-286
686 Parsons AJ, Foster IDL (2011) What can we learn about soil erosion from the use of 137Cs?
687 Earth-Sci Rev 108:101-113
688 Quénard L, Samouelian A, Laroche B, Cornu S (2011) Lessivage as a major process of soil
689 formation: A revisitation of existing data. Geoderma 167-168:135-147
690 Ritchie JC, Ritchie CA (2007) Bibliography of publications of 137cesium studies related to
691 erosion and sediment deposition. Tech. rep., USDA Agricultural Research Service
692 Rosén K, Öborn I, Lönsjö H (1999) Migration of radiocaesium in Swedish soil profiles after
693 the Chernobyl accident, 1987–1995. J Environ Radioact 46:45-66
694 Sanchez A, Smolders E, Van den Brande K, Merckx R, Wright S, Naylor C (2002)
695 Predictions of in situ solid/liquid distribution of radiocaesium in soils. J Environ
696 Radioact 63:35-47
697 Sawhney B (1972) Selective sorption and fixation of cations by clay minerals: a review. Clays

698 Clay Miner 20:93-100
699 Schiffers K, Teal LR, Travis JMJ, Solan M (2011) An open source simulation model for soil
700 and sediment bioturbation. PloS ONE 6:e28028
701 SchimmackW, Márquez FF (2006) Migration of fallout radiocaesium in a grassland soil from
702 1986 to 2001. Part II: Evaluation of the activity-depth profiles by transport models. Sci
703 Total Environ 368:863-874
704 Schimmack W, Schultz W (2006) Migration of fallout radiocaesium in a grassland soil from
705 1986 to 2001 - Part I: Activity-depth profiles of Cs-134 and Cs-137. Sci Total Environ
706 368:853-862
707 Schuller P, Bunzl K, Voigt G, Ellies A, Castillo A (2004) Global fallout Cs-137 accumulation
708 and vertical migration in selected soils from South Patagonia. J Environ Radioactiv
709 71:43-60
710 Schuller P, Ellies A, Kirchner G (1997) Vertical migration of fallout Cs-137 in agricultural
711 soils from Southern Chile. Sci Total Environ 193:197-205
712 Sigurgeirsson MA, Arnalds O, Palsson SE, Howard BJ, Gudnason K (2005) Radiocaesium
713 fallout behaviour in volcanic soils in Iceland. J Environ Radioact 79:39-53
714 Smith JT, Elder DG (1999) A comparison of models for characterizing the distribution of
715 radionuclides with depth in soils. Eur J Soil Sci 50:295-307
716 Smith JT, Fesenko SV, Howard BJ, Horrill AD, Sanzharova NI, Alexakhin RM, Elder DG,
717 Naylor C (1999) Temporal change in fallout 137Cs in terrestrial and aquatic systems:
718 a whole ecosystem approach. Environ Sci Tech 33:49-54
719 Szerbin P, Koblinger-Bokori E, Koblinger L, Vegvari I, Ugron A (1999) Caesium- 137
720 migration in Hungarian soils. Sci Total Environ 227:215-227
721 Soil Survey Staff (1999) Soil taxonomy: a basic system of soil classification for making and
722 interpreting soil surveys. US Department of Agriculture, Agriculture Handbook, N°

436, Washington DC, 2nd edition

Tamura T, Jacobs D (1960) Structural implications in cesium sorption. Health Phys 2:391-398

Turner NB, Ryan JN, Saiers JE (2006) Effect of desorption kinetics on colloid facilitated transport of contaminants: Cesium, strontium, and illite colloids. Water Resour Res 42:W12S09

Tyler A, Carter S, Davidson D, Long D, Tipping R (2001) The extent and significance of bioturbation on Cs-137 distributions in upland soils. Catena 43:81-99

UNSCEAR (1982) Ionizing radiation: sources and biological effects report to the general assembly, with annexes. Tech. rep., United Nations, New York

Vandebroek L, Van Hees M, Delvaux B, Spaargaren O, Thiry Y (2012) Relevance of Radiocaesium Interception Potential (RIP) on a worldwide scale to assess soil vulnerability to ^{137}Cs contamination. J Environ Radioact 104:87-93

VandenBygaart A, Protz R, Tomlin A, Miller J (1998) Cs-137 as an indicator of earthworm activity in soils. Appl Soil Ecol 9:167-173

Wilkinson MT, Richards PJ, Humphreys GS (2009) Breaking ground: Pedological, geological, and ecological implications of soil bioturbation. Earth Sci Rev 97:257-272

Zhang X, Long Y, He X, Fu J, Zhang Y (2008) A simplified (CS)-C-137 transport model for estimating erosion rates in undisturbed soil. J Environ Radioactiv 99:1242-1246

Zhang X, Qi Y, Walling DE, He X, Wen A, Fu J (2006) A preliminary assessment of the potential for using Pb-210(ex) measurement to estimate soil redistribution rates on cultivated slopes in the Sichuan Hilly Basin of China. Catena 68:1-9

Zheng JJ, He XB, Walling D, Zhang XB, Flanagan D, Qi YQ (2007) Assessing soil erosion rates on manually-tilled hillslopes in the Sichuan Hilly Basin using Cs-137 and Pb-210(ex) measurements. Pedosphere 17:273-283

Table 1 Studies and soil profiles contained in the database and their main characteristics

WRB soil groups	Landuse or cover	Country	Sampling year	Nb of profiles	Inventory range Bq m^{-2}	Profil-class	Climate Köppen-Geiger classification	OM[a] range %	pH range	Paper
Acrisol	Grassland	China	2004	1	1300	2	Cwa	NA	NA	Zhang et al. (2008)
Arenosol	Forest	Germany	1999	1	36123	4	Cfb	6.3	7.7	Kruse-Irmer and Giani (2003)
	Grassland	Serbia	2001	1	11523	5	Cfb	3.3	5.2	Krstic et al. (2004)
Cambisol	Forest	Germany	1998-99	3	1465-28452	1	Cfb	6.2-19.6	4.1-4.4	Kruse-Irmer and Giani (2003)
	Grassland	Syria	2000	2	2814-6420	1; 5	Csa	NA	NA	Al-Masri (2006)
		Sweden	1998	1	1927	3	Cfb	NA	NA	Isaksson et al. (2001)
		Sweden	2007	1	55950	6	Dfb	22.0	5.2	Jarvis et al. (2010)
		Serbia	2001	4	9947-17842	3; 4; 6	Cfb	5.8-8.8	5.2-5.9	Krstic et al. (2004)
		Germany	1999	1	26302	4	Cfb	9.1	6.3	Kruse-Irmer and Giani (2003)
		Spain	2006	1	2771	6	Csb	NA	NA	Legarda et al. (2011)
		Sweden	1994	1	75147	3	Dfb	22.0	5.2	Rosen et al. (1999)
		Hungary	1995-97	7	2200-13500	1; 3; 4	Cfb	1.1-8.2	5.6-7.5	Szerbin et al. (1999)
Chernozem	Grassland	Hungary	1995	2	4200-6100	3; 6	Cfb	3.4-4.4	7.2-8.1	Szerbin et al. (1999)
Fluvisol	Grassland	Serbia	2001	2	4595-20632	3; 5	Cfb	1.0-7.3	4.8-7.0	Krstic et al. (2004)
		Hungary	1995	5	1300-7800	3; 4	Cfb	0.9-5.0	6.2-7.9	Szerbin et al. (1999)
Histosol	Forest	Germany	1998	1	5040	3	Cfb	93.0	4.0	Kruse-Irmer and Giani (2003)
	Grassland	Germany	1999	1	53712	1	Cfb	78.9	4.4	Kruse-Irmer and Giani (2003)
		Sweden	2007	1	111400	6	Dfb	46.3	5.9	Matisoff et al. (2011)[b]
		Sweden	1994	2	53463-165913	3	Dfb	64.6	5.5	Rosen et al. (1999)
	Peat	Ireland	NA[a]	2	3900-4800	5	Cfb	NA	NA	Gallagher et al. (2001)
Leptosol	Grassland	Hungary	1995-97	2	6000-21500	1; 4	Cfb	2.0-4.6	7.7-7.8	Szerbin et al. (1999)

Luvisol	Forest	Canada	NA	1	1610	6	Dfb	NA	7.7	Milton et al. (2001)
	Grassland	Syria	2000	2	2218-9647	1; 3	Csa	NA	NA	Al-Masri (2006)
		Germany	2001	5	18161-23640	3; 5	Cfb	12.4	NA	Schimmack and Schultz (2006)
Phaeozem	Grassland	Sweden	1992	1	159923	3	Dfb	1.1	6.2	Rosen et al. (1999)
Podzol	Forest	Canada	NA	1	3030	3	Dfb	NA	4.9	Milton et al. (2001)
	Grassland	Sweden	1994	1	2921	6	Dfc	3.0	4.9	Rosen et al. (1999)
Regosol	Cultivated	China	2002	3	898-1840	7	Cwa	NA	NA	Zhang et al. (2006)
	Forest	Turkey	2002	16	2974-21201	1; 2; 5; 6	Csa	3.8-11.0	5.1-7.5	Karadeniz and Yaprak (2008)
		Germany	1999	1	23486	2	Cfb	3.8	7.7	Kruse-Irmer and Giani (2003)
	Grassland	Germany	1999	1	50642	2	Cfb	8.4	7.4	Kruse-Irmer and Giani (2003)
		Sweden	1994-95	3	11214-47230	1; 3; 5	Dfc	7.2-7.5	5.4-6.3	Rosen et al. (1999)
		China	2002	1	1984	2	Cwa	NA	NA	Zhang et al. (2006)
		China	2004	1	2244	6	Cwa	NA	NA	Zheng et al. (2007)
Solonetz	Grassland	Hungary	1995-97	3	1300-4400	1; 4	Cfb	2.1-4.6	6.3-7.4	Szerbin et al. (1999)
Vertisol	Cultivated	Morocco	NA	1	952	7	Csa	NA	NA	Mabit et al. (2008)
	Grassland	Syria	2000	1	5646	4	Csa	NA	NA	Al-Masri (2006)
		Serbia	2001	3	12104-19975	2; 4	Cfb	3.9-6.0	5.7-7.5	Krstic et al. (2004)
		Morocco	NA	1	1445	3	Csa	NA	NA	Mabit et al. (2008)
Yermosol	Grassland	Syria	2000	7	2000-6477	1; 3; 4; 6	BSh; BSk; BWk	NA	NA	Al-Masri (2006)

[a] OM stands for organic matter and NA for not analysed (or probived)
[b] Four other profiles from this study were excluded as we were not able to determine the soil bulk density with the soil bulk density model and the inventories reported in the paper (negative values)

Table 2 Values of global ^{137}Cs fallout estimated by UNSCEAR (1982) for different ranges of latitude and simulated in this study for the different modelled sites (grouped according to their latitude)

Latitude band	Estimation UNSCEAR[a]	r_{th}	Global fallout values simulated: mean [range]
(degrees)	Bq m^{-2}		Bq m^{-2}
60-70	2425	0.80	3999 [3954 - 4044] (n=2)
50-60	4028	1.34	3205 [815 - 4044] (n=9)
40-50	4502	1.50	3561 [0 - 4527] (n=44)
30-40	3261	1.09	1358 [0 - 3289] (n=13)
20-30	2467	0.82	2806 [1931 - 3531][b] (n=3)

[a]: calculated as ^{90}Sr deposition published in (UNSCEAR, 1982) times 1.6 (ratio $^{137}Cs/^{90}Sr$ in global fallout) and decay-corrected for 1986

[b]: sites located in China (~29°N) hypothesized to be free of Chernobyl contamination

Table 3 Types of profile depth distributions attributed to the different soil groups

Profile depth distribution	Type 1	Type 2	Type 3	Type 4	Type 5	Type 6	Type 7
Acrisols	0	1	0	0	0	0	0
Arenosols	0	0	0	1	1	0	0
Cambisols	5	0	7	5	1	3	0
Chernozems	0	0	1	0	0	1	0
Fluvisols	0	0	4	2	1	0	0
Histosols	1	0	3	0	2	1	0
Leptosols	1	0	0	1	0	0	0
Luvisols	0	0	4	0	2	1	0
Phaeozems	0	0	1	0	0	0	0
Podzols	0	0	1	0	0	1	0
Regosols	2	6	1	0	5	9	3
Solonetz	2	0	0	1	0	0	0
Vertisols	0	2	1	2	0	0	1
Yermosols	3	0	1	1	0	3	0

Table 4 Types of profile depth distributions collected under different climates

Climate type	Class[a]	Type 1	Type 2	Type 3	Type 4	Type 5	Type 6	Type 7
Cold desert climate	BWk	1	0	0	0	0	0	0
Warm steppe climate	BSh	1	0	0	1	0	2	0
Cold steppe climate	BSk	1	0	1	0	0	1	0
Temperate climate	Cfb	8	4	15	11	6	2	0
	Csa	2	3	2	1	5	8	1
	Csb	0	0	0	0	0	1	0
	Cwa	0	2	0	0	0	1	3
Continental climate	Dfb	0	0	5	0	0	3	0
	Dfc	1	0	1	0	1	1	0

[a] Köppen-Geiger climate classes determined according to Kottek et al. (2006).
Main climate: B- Arid, C- Warm Temperate, D- Snow
Precipitation: W- desert, S- steppe, f- fully humid, s-summer dry, w- winter dry
Temperature: h- hot arid, k-cold arid, a- hot summer, b- warm summer, c- cool summer

Table 5 Average and associated standard deviation of the diffusion coefficient (D_s), the convection velocity (v_s) and the mean migration depth of a Dirac distribution after 25 years for the different soil groups compiled in the database

Soil type	n	D_s $cm^2\ yr^{-1}$	v_s $cm\ yr^{-1}$	*Migration depth cm*
Acrisols	1	1.52	0.00	6.96
Arenosols	2	1.98±0.67	0.13±0.12	7.33±0.02
Cambisols	19	0.96±0.85	0.11±0.13[ab]	6. 81±3.06
Chernozems	2	1.06±0.95	0.46±0.29	13.42±8.05
Fluvisols	7	1.16±1.50	0.18±0.14[ab]	8.34±2.73
Histosols	7	1.33±1.51	0.22±0.26[ab]	9.86±4.16
Leptosols	2	1.37±1.61	0.22±0.30	9.18±9.16
Luvisols	7	0.41±0.18	0.22±0.06[a]	7.31±0.88
Phaeozems	1	0.08	0.16	4.53
Podzols	1	0.09	0.06	2.60
Regosols	6	0.60±0.40	0.10±0.12[ab]	5.76±1.73
Solonetz	3	0.89±0.69	0.03±0.05	5.36±2.69
Vertisols	5	1.18±0.67	0.05±0.04[b]	6.56±1.59
Yermosols	8	0.84±0.86	0.19±0.19[ab]	7.43±5.67

a, ab, b: ANOVA analysis performed for soil groups with more than 3 individuals with a Fisher test at 5 % of confidence level. The ANOVA could not discriminate groups with the Fisher test for D_s and *migration depth*.

Figure captions

Fig. 1: Modelling of soil bulk densities: (a) Linear regression of mean bulk densities (open circles) and bulk density profiles (lines) documented in the database (n=13); error bars represent standard deviation in the data, (b) Comparison of simulated bulk densities with the bulk densities documented in the database

Fig. 2: The different depth-distribution profile types for ^{137}Cs compiled in the database. Typical examples are provided. The distributions were normalized by their maximum concentrations. Type 1: example of profile CMg of Kruse-Irmer and Giani (2003); type 2: example of the reference profile of Zhang et al. (2008); type 3: example of Möjsjövik from Rosen et al. (1999); type 4: example of Somogy from Szerbin et al. (1999); type 5: example of profile E from Schimmack and Schultz (2006)); type 6: example of Veszprém from Szerbin et al. (1999).

Fig. 3: Simulated versus observed ^{137}Cs values in the entire set of modeled profiles

Fig. 4: Scaled residuals (n=809) of all simulations and its moving average as a function of soil depth. Note that the moving average of the scaled residuals shifted towards positive values below 13 cm and that the scaled residuals remained systematically positive below 30 cm

Fig. 5: Relationship between fitted diffusion and convection velocity coefficients for selected soils groups: a, Yermosols; b, Cambisols; c, Luvisols; d, Regosols

Fig. 6: Relationship between fitted convection velocity and time after the main ^{137}Cs input (i.e., global fallout and Chernobyl accident)

Figure 1

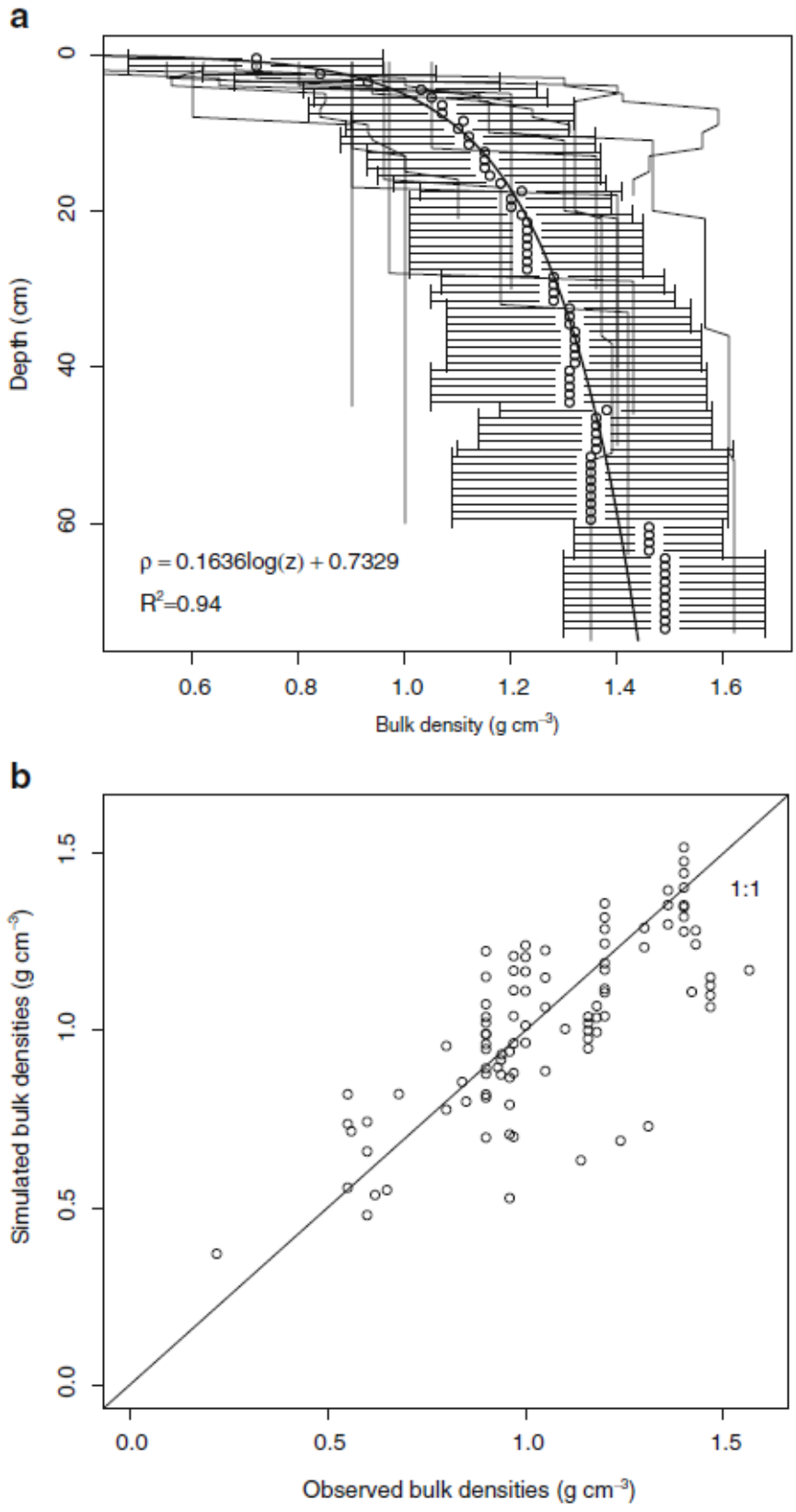
a
Depth (cm)
0
20
40
60
ρ = 0.1636log(z) + 0.7329
R²=0.94
0.6
0.8
1.0
1.2
1.4
1.6
Bulk density (g cm⁻³)
b
Simulated bulk densities (g cm⁻³)
0.0
0.5
1.0
1.5
1:1
0.0
0.5
1.0
1.5
Observed bulk densities (g cm⁻³)

Figure 2.

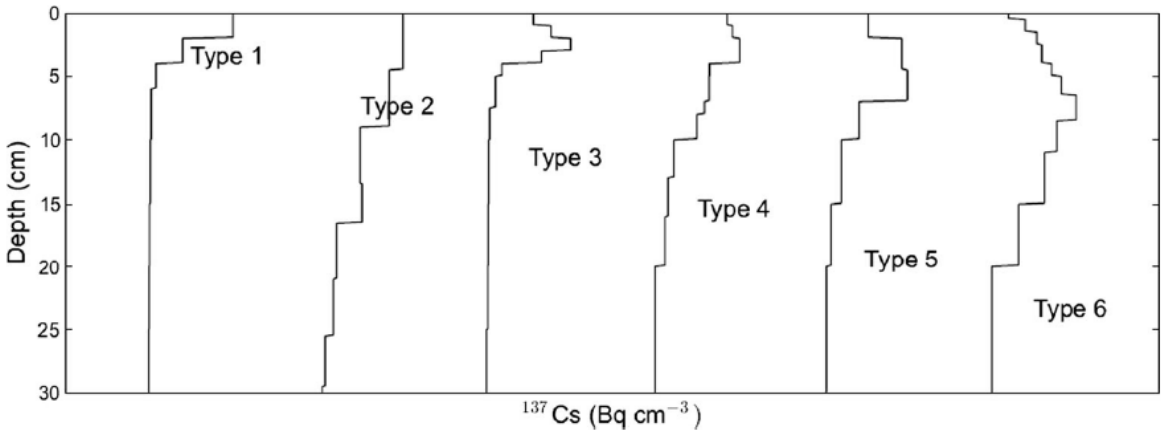
Type 1
Type 2
Type 3
Type 4
Type 5
Type 6
Depth (cm)
0
5
10
15
20
25
30
^{137}Cs (Bq cm^{-3})

Figure 3.

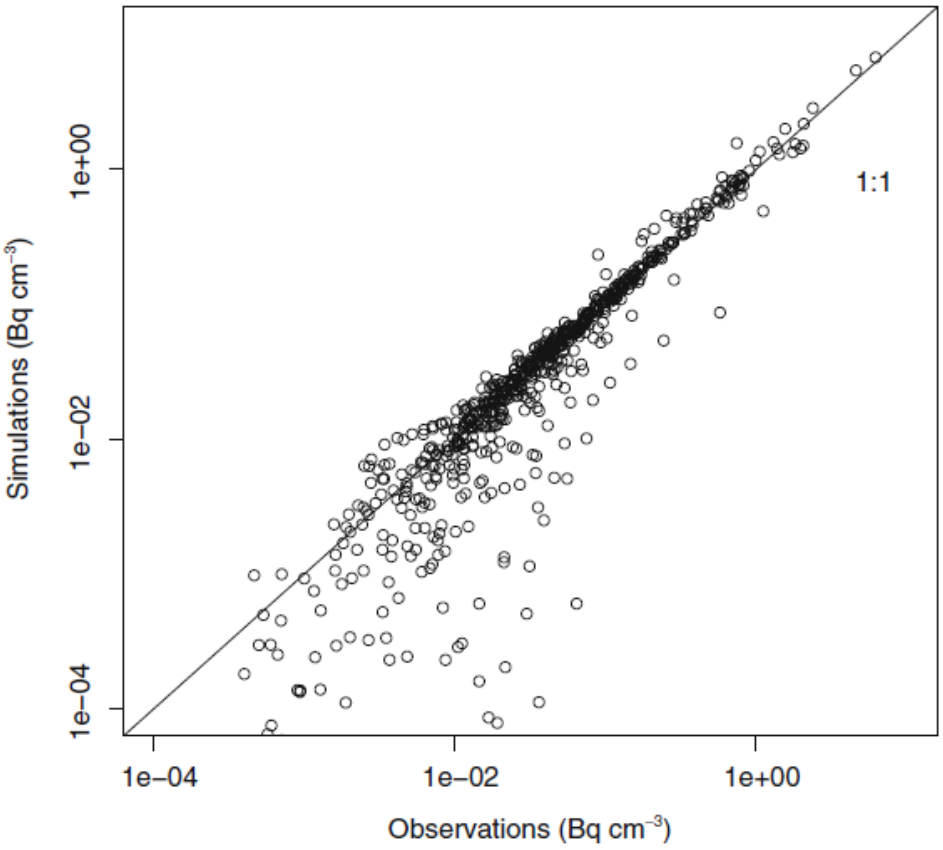
1:1
Simulations (Bq cm^{-3})
1e−04
1e−02
1e+00
Observations (Bq cm^{-3})
1e−04
1e−02
1e+00

Figure 4.

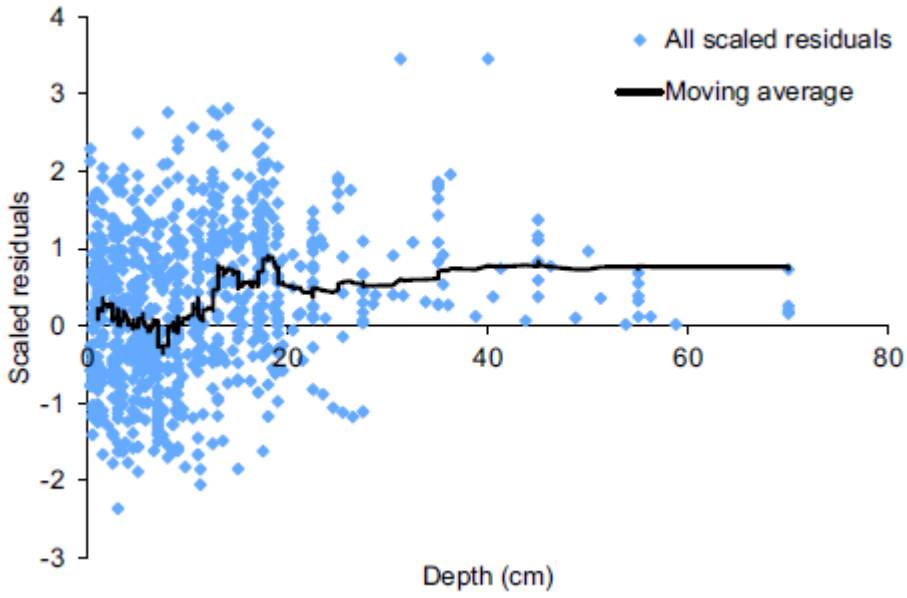
All scaled residuals
Moving average
Scaled residuals
Depth (cm)
4
3
2
1
0
-1
-2
-3
0
20
40
60
80

Figure 5.

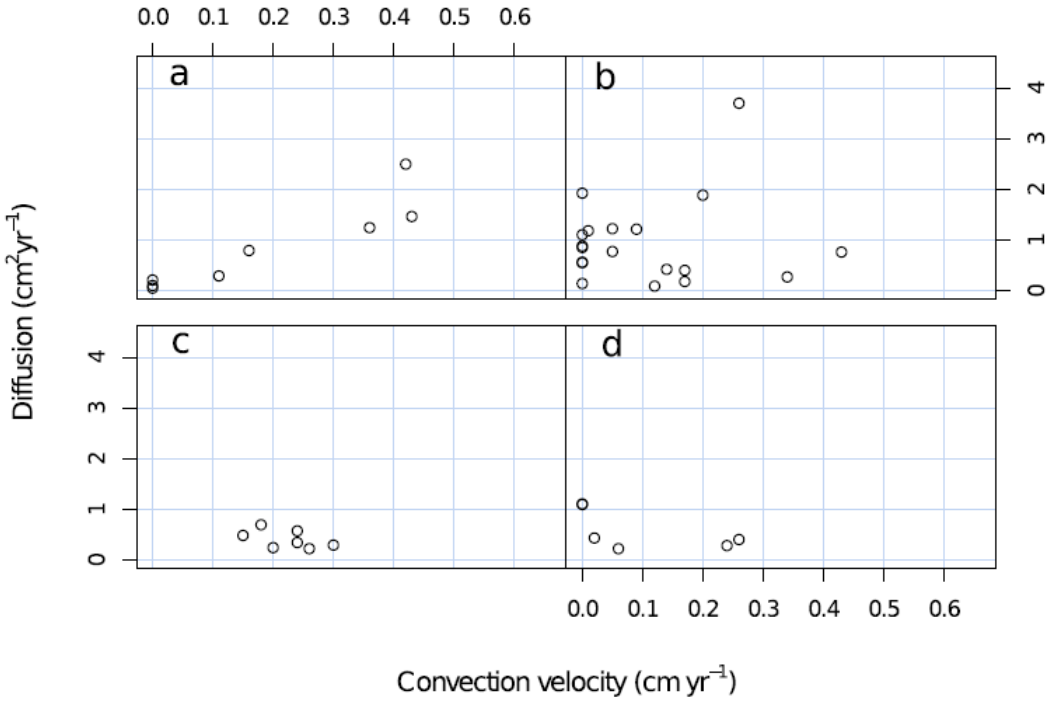
a
b
c
d
Diffusion (cm²yr⁻¹)
Convection velocity (cm yr⁻¹)
0.0
0.1
0.2
0.3
0.4
0.5
0.6
0
1
2
3
4

Figure 6.

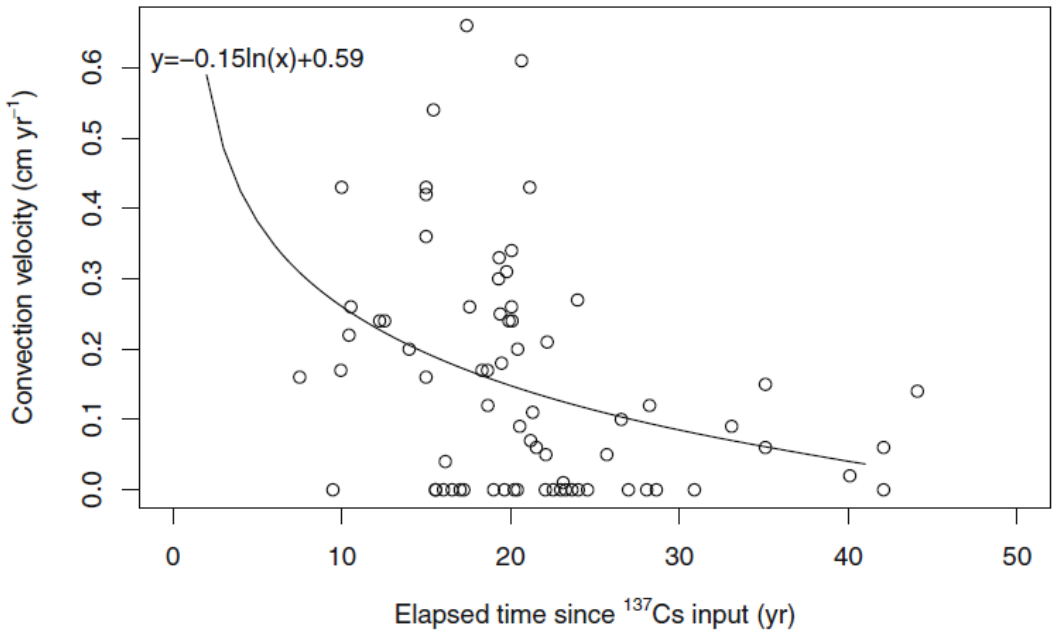
y=−0.15ln(x)+0.59
Convection velocity (cm yr^{-1})
0.0
0.1
0.2
0.3
0.4
0.5
0.6
0
10
20
30
40
50
Elapsed time since ^{137}Cs input (yr)